Extension of Numerical Matching Method to Weakly Nonlinear Evolution of Resistive MHD Modes

Masaru FURUKAWA and Shinji TOKUDA[1)]

Graduate School of Engineering, Tottori University, Tottori-shi, Tottori 680-8552, Japan
[1)]*Research Organization for Information Science and Technology, Shinagawa-ku, Tokyo 140-0001, Japan*

(Received 14 March 2017 / Accepted 1 May 2017)

We have extended "numerical matching method" to weakly nonlinear regime, which is relevant for the Rutherford regime of magnetic island evolution in normal magnetic shear plasmas as well as for reversed magnetic shear plasmas to which the Rutherford theory does not apply. The numerical matching method was developed for linear stability analyses of resistive magnetohydrodynamics (MHD) modes by utilizing an inner region with a finite width, that removes difficulties inherent in its numerical applications of the traditional matched asymptotic expansion. The extended method is applied to low-beta reduced MHD simulations of magnetic island evolution in cylindrical plasmas with normal and reversed magnetic shear profiles. The numerical results agree well with fully nonlinear simulation without using the matching method from the linear to weakly nonlinear regimes continuously. Since the nonlinear equation is solved only in the inner region of a finite width, the computational cost is reduced, which enables us to include more detailed physics effects. Our extended method therefore makes a significant contribution in the MHD analysis of magnetic island evolution beyond the restriction in the conventional Rutherford theory.

Keywords: magnetic island, nonlinear theory, matched solution using finite-width inner region, resistive magnetohydrodynamics

DOI: 10.1585/pfr.12.1403025

1. Introduction

The theory of matched asymptotic expansion for linearized resistive magnetohydrodynamics (MHD) is well established [1]. After ten years of this pioneering work, the theory was extended to nonlinear regime [2]. Since then many applications of the Rutherford equation [2] have made much progress in fusion research, especially in the neoclassical tearing mode (NTM) studies [3–5]. Besides many numerical studies performed, the theoretical framework has been always based on the Rutherford equation essentially.

We have recently developed a new framework for the linear stability analyses of resistive MHD modes, i.e. the numerical matching method [6–8]. This method utilizes a finite-width inner region around a resonant surface, where the resistive MHD is solved, instead of an infinitely thin inner layer as in the traditional matched asymptotic expansion. The reason why we adopt a finite-width inner region is because it can remove difficulties inherent in numerical applications of the matched asymptotic expansion. For example, it is not easy to precisely compute the ratio of the diverging big to small solutions around the resonant surface numerically, which is required for the matched asymptotic expansion, although sophisticated theories have been developed [9–12]. By using the inner region with a finite width, we do not need to compute the ratio of the big to small solutions for the matching. Instead, we need an appropriate boundary condition for the direct matching across the interfaces between the outer and inner regions. In [6], we developed such a boundary condition for the reduced MHD [13, 14]. The important point is to impose a boundary condition such that the electric field along the magnetic field smoothly disappears as approaching from inner to outer regions. We developed both an eigenvalue and an initial-value approaches. In [7], another boundary condition was developed, which enables us to include inertia correction perturbatively to the outer solutions. Then the stability analysis of high beta plasmas has become possible even if the plasma is close to its marginal stability. The diamagnetic drift effect was also taken into account by the inclusion of the inertia correction to the outer solution [8].

In this paper, we extend the initial-value approach of the numerical matching method to weakly nonlinear regime. Namely, the nonlinear evolution equation is solved in the finite-width inner region, while the inertia-less linearized ideal MHD equation, or the Newcomb equation [15], is solved in the outer region. Then the solutions are matched at the interfaces between the outer and inner regions. This is the situation assumed in the Rutherford theory [2]. In Sec. 2, we firstly explain the setting of the problem. The low-beta reduced MHD [13] is adopted for cylindrical plasmas in this paper. We then develop the solution

author's e-mail: furukawa@damp.tottori-u.ac.jp

method for both the inner and outer regions as well as the matching condition. In Sec. 3, we show numerical results by the developed method. The first one is the Rutherford regime of magnetic island evolution in a normal magnetic shear plasma, while the second one is the nonlinear evolution of double tearing mode in a reversed magnetic shear plasma. Both results agree well with fully nonlinear simulation without the matching method. In Sec. 4, we discuss four topics; namely, the importance of equilibrium components in the numerical results, the reduction of computational cost, the significance of the application to the reversed magnetic shear cases, and possible application to the high-beta toroidal plasmas. Then conclusions are given in Sec. 5.

2. Theory

2.1 Setting

In this study, we adopt the low-beta reduced MHD [13] in the cylindrical geometry as the simplest situation for demonstrating the principal ideas of our method. Let us consider a cylindrical plasma with minor radius a and length $2\pi R_0$. The cylindrical coordinates are (r, θ, z). A toroidal angle $\zeta := z/R_0$ is also used instead of the axial coordinate z. The inverse aspect ratio is given by $\varepsilon := a/R_0$. Physical quantities are normalized by the length a, the magnetic field in the z-direction B_0, the Alfvén velocity $v_\mathrm{A} := B_0/\sqrt{\mu_0\rho_0}$ with μ_0 and ρ_0 being vacuum permeability and typical mass density, respectively, and the Alfvén time $\tau_\mathrm{A} := a/v_\mathrm{A}$. Then the low-beta reduced MHD equations are

$$\frac{\partial U}{\partial t} = [U, \varphi] + [\psi, J] - \varepsilon\frac{\partial J}{\partial \zeta}, \tag{1}$$

$$\frac{\partial \psi}{\partial t} = [\psi, \varphi] - \varepsilon\frac{\partial \varphi}{\partial \zeta} + \eta J. \tag{2}$$

Here, the fluid velocity is given by $\boldsymbol{v} = \hat{\mathbf{z}} \times \nabla\varphi$, and the magnetic field by $\boldsymbol{B} = \hat{\mathbf{z}} + \nabla\psi \times \hat{\mathbf{z}}$. The unit vector in the z direction is denoted as $\hat{\mathbf{z}}$. The vorticity in the z direction is $U := \triangle_\perp\varphi$, where $\triangle_\perp$ is the Laplacian in the r–θ plane. The current density in the z direction multiplied by a negative sign is given by $J := \triangle_\perp\psi$. The Poisson bracket for two functions f and g is defined by $[f, g] := \hat{\mathbf{z}} \cdot \nabla f \times \nabla g$. The inverse of the Lundquist number is denoted by η. Equation (1) is the vorticity equation, and Eq. (2) is the parallel Ohm's law.

Let us write the vector of the fields as $\boldsymbol{u}(\boldsymbol{x}, t) := (\varphi(\boldsymbol{x}, t), \psi(\boldsymbol{x}, t))^\mathrm{T}$, and let us assume $\boldsymbol{u} = \boldsymbol{u}_0(\boldsymbol{x}) + \boldsymbol{u}_1(\boldsymbol{x}, t)$ with $\boldsymbol{u}_0 = (0, \psi_0(r))^\mathrm{T}$ and $\boldsymbol{u}_1 = (\varphi_1(\boldsymbol{x}, t), \psi_1(\boldsymbol{x}, t))^\mathrm{T}$. Namely, the equilibrium is cylindrically symmetric, and has no plasma rotation. The time-dependent part $\boldsymbol{u}_1$ is not necessarily small. Then the governing Eqs. (1) and (2) can be written in the following form:

$$\mathcal{M}\frac{\partial \boldsymbol{u}_1}{\partial t} = \mathcal{L}\boldsymbol{u}_1 + \boldsymbol{N}(\boldsymbol{u}_1), \tag{3}$$

where the explicit expressions for the the linear operators $\mathcal{M}$ and $\mathcal{L}$, and the nonlinear term $\boldsymbol{N}(\boldsymbol{u}_1)$ are

$$\mathcal{M} = \begin{pmatrix} \triangle_\perp & 0 \\ 0 & 1 \end{pmatrix}, \tag{4}$$

$$\mathcal{L} = \begin{pmatrix} 0 & [\psi_0, \triangle_\perp\ ] - [J_0,\ ] - \varepsilon\dfrac{\partial(\triangle_\perp\ )}{\partial\zeta} \\ [\psi_0,\ ] - \varepsilon\dfrac{\partial}{\partial\zeta} & \eta\triangle_\perp \end{pmatrix}, \tag{5}$$

$$\boldsymbol{N}(\boldsymbol{u}_1) = \begin{pmatrix} [U_1, \varphi_1] + [\psi_1, J_1] \\ [\psi_1, \varphi_1] \end{pmatrix}. \tag{6}$$

We set an inner region at $r_\mathrm{L} < r < r_\mathrm{R}$, which covers resonant surfaces of the mode under consideration. The outer region is the complement of the union of the inner region and the boundaries, given by $0 \le r < r_\mathrm{L}$ and $r_\mathrm{R} < r < 1$. Thus the interfaces are $r = r_\mathrm{R}$ and $r = r_\mathrm{L}$. Extensions to multiple inner regions would be straightforward.

2.2 Outer region

In the outer region, we solve the inertia-less, linearized ideal MHD equation or the Newcomb equation, which is given by the first row of $\mathcal{L}\boldsymbol{u}_1 = 0$. Since the geometry is cylindrical, we decompose the fields in a Fourier series as

$$\begin{aligned}\boldsymbol{u}_1 &= \sum_{m,n} \boldsymbol{u}_{mn}(r, t)\mathrm{e}^{\mathrm{i}(m\theta - n\zeta)} \\ &= \sum_{m,n} \begin{pmatrix} \tilde{\varphi}_{mn}(r, t) \\ \tilde{\psi}_{mn}(r, t) \end{pmatrix} \mathrm{e}^{\mathrm{i}(m\theta - n\zeta)},\end{aligned} \tag{7}$$

where m and n are poloidal and toroidal mode numbers, respectively. The Newcomb equation is given by

$$\begin{aligned}\mathcal{N}\tilde{\psi}_{mn} &:= \left\{\frac{1}{r}\frac{\partial}{\partial r}\left(r\frac{\partial}{\partial r}\right) - \left(\frac{m}{r}\right)^2\right\}\tilde{\psi}_{mn} + \frac{mJ_0'(r)}{rk_\parallel}\tilde{\psi}_{mn} \\ &= 0,\end{aligned} \tag{8}$$

where $\mathcal{N}$ is the Newcomb operator and

$$k_\parallel(r) := \varepsilon m\left(\frac{1}{q} - \frac{n}{m}\right). \tag{9}$$

The prime denotes r derivative, and the safety factor is given by $q(r) = -\varepsilon r/\psi_0'(r)$. Equation (8) is the second-order, linear ordinary differential equation for $\tilde{\psi}_{mn}$, and can be solved independently for each pair of m and n. The solution can be expressed as a linear combination of two independent solutions. Let us construct the solution by Green's functions defined by

$$\begin{aligned}&\mathcal{N}G^\psi_{\mathrm{out},mn,p}(r) = 0, \\ &\quad G^\psi_{\mathrm{out},mn,p}(r_q) = \delta_{pq}, \qquad p, q = \text{ L or R}.\end{aligned} \tag{10}$$

Namely, the amplitude of $G^\psi_{\mathrm{out},mn,p}(r)$ is unity at $r = r_p$, and is zero at the other side of the outer region. If one of the boundaries is the magnetic axis, the regularity condition

is imposed and thus one of the two independent solutions drops. At the plasma edge, we assume the fixed-boundary condition that also drops one of the two independent solutions. These are similarly imposed even if the magnetic axis or the plasma edge is in the inner regions. Now we express the outer solution as

$$\tilde{\psi}_{mn}(r,t) = \sum_{p=\mathrm{L,R}} \tilde{\psi}_{mn,p}(t) G^{\psi}_{\mathrm{out},mn,p}(r). \tag{11}$$

We have included time dependence in the coefficients $\tilde{\psi}_{mn,p}(t)$, which must be slow. From the outer region itself, there is no way to determine $\tilde{\psi}_{mn,p}(t)$. It will be determined through the matching condition with the inner solution in Sec. 2.4.

2.3 Inner region

In the inner region, we solve the nonlinear evolution Eq. (3). Let us discretize time with a constant interval h, and denote the discrete time as t^i with i being an index. Similarly, we write $\boldsymbol{u}^i := \boldsymbol{u}(t^i)$. If we adopt the Kth-order Adams–Moulton method ($K = 1, 2, \cdots$), an unknown $\boldsymbol{u}^{i+1}$ is calculated by

$$\mathcal{M}\boldsymbol{u}^{i+1} = \mathcal{M}\boldsymbol{u}^i + h \sum_{k=2-K}^{1} c_k \left(\mathcal{L}\boldsymbol{u}^{i+k} + \boldsymbol{N}(\boldsymbol{u}^{i+k}) \right), \tag{12}$$

where c_ks are known constants. For example, $c_1 = 1$ for $K = 1$, which is the simplest implicit method as developed in [6]. It is extended to higher orders $K \geq 2$ here. For $K = 2$, $c_0 = c_1 = \frac{1}{2}$. The constants for $K \geq 3$ are found in standard textbooks.

We rewrite Eq. (12) by moving the term linear in $\boldsymbol{u}^{i+1}$ to the left-hand side and by separating out the nonlinear term of $\boldsymbol{u}^{i+1}$ from the summation as

$$\begin{aligned}(\mathcal{M} - c_1 h\mathcal{L})\,\boldsymbol{u}^{i+1} &= \mathcal{M}\boldsymbol{u}^i \\ &+ h \sum_{k=2-K}^{0} c_k \left(\mathcal{L}\boldsymbol{u}^{i+k} + \boldsymbol{N}(\boldsymbol{u}^{i+k}) \right) + c_1 h \boldsymbol{N}(\boldsymbol{u}^{i+1}).\end{aligned} \tag{13}$$

Then the last nonlinear term is unknown, while the remainings on the right-hand side are known. Thus we need an iteration for the last term to solve this equation. Therefore we introduce the following expression for the inner solution

$$\begin{aligned}\boldsymbol{u}^{i+\frac{j}{J}}_{mn}(r) &= \sum_{p=\mathrm{L,R}} \tilde{\psi}^{i+\frac{j}{J}}_{mn,p} \boldsymbol{G}_{\mathrm{in},mn,p}(r) + \boldsymbol{H}^{i+\frac{j}{J}}_{\mathrm{in},mn}(r), \\ & j = 0, 1, \cdots, J,\end{aligned} \tag{14}$$

where J is the maximum number of the iteration, and we assume that $\boldsymbol{u}^{i+\frac{j}{J}}_{mn}(r)$ becomes sufficiently close to $\boldsymbol{u}^{i+\frac{j-1}{J}}_{mn}(r)$ when $j = J$. The Green's functions $\boldsymbol{G}_{\mathrm{in},mn,p}(r) = (G^{\varphi}_{\mathrm{in},mn,p}(r), G^{\psi}_{\mathrm{in},mn,p}(r))^{\mathrm{T}}$ is given by

$$\begin{aligned}(\mathcal{M} - c_1 h\mathcal{L})\,\boldsymbol{G}_{\mathrm{in},mn,p}(r) &= 0, \\ G^{\psi}_{\mathrm{in},mn,p}(r_q) &= \delta_{pq}, \qquad p, q = \mathrm{L \text{ or } R}.\end{aligned} \tag{15}$$

The boundary condition for the φ component of the Green's function, $G^{\varphi}_{\mathrm{in},mn,p}(r)$, was developed in [6], and is given such that the parallel electric field disappears smoothly as approaching from the inner to the outer regions. We need to calculate these Green's functions only once at the beginning of the simulation because $\mathcal{M}$ and $\mathcal{L}$ do not change during the time evolution. Also the inhomogeneous solution $\boldsymbol{H}^{i+\frac{j}{J}}_{\mathrm{in},mn}(r) = (H^{\varphi,i+\frac{j}{J}}_{\mathrm{in},mn}(r), H^{\psi,i+\frac{j}{J}}_{\mathrm{in},mn}(r))^{\mathrm{T}}$ is obtained by solving

$$\begin{aligned}(\mathcal{M} - c_1 h\mathcal{L})\,\boldsymbol{H}^{i+\frac{j}{J}}_{\mathrm{in},mn}(r) &= \mathcal{M}\boldsymbol{u}^i_{mn}(r) \\ &+ h \sum_{k=2-K}^{0} c_k \left(\mathcal{L}\boldsymbol{u}^{i+k}_{mn} + \boldsymbol{N}_{mn}(\boldsymbol{u}^{i+k}) \right) + c_1 h \boldsymbol{N}_{mn}(\boldsymbol{u}^{i+\frac{j-1}{J}}), \\ H^{\psi,i+\frac{j}{J}}_{\mathrm{in},mn}(r_p) &= 0, \qquad p = \mathrm{L \text{ and } R},\end{aligned} \tag{16}$$

for $j = 1, \cdots, J$, where $\boldsymbol{N}_{mn}$ is the Fourier coefficient of $\boldsymbol{N}(\boldsymbol{u})$. The boundary condition for $H^{\varphi,i+\frac{j}{J}}_{\mathrm{in},mn}$ is again the smooth disappearance of parallel electric field, as same as the Green's functions. The iteration must be performed together with the determination of the amplitudes $\tilde{\psi}^{i+\frac{j}{J}}_{mn,p}$ described in the next subsection.

2.4 Matching condition

In the numerical matching method, we impose continuity of ψ and its radial derivatives at the interfaces. First let us take $\tilde{\psi}_{mn,p}(t)$ in the outer region equal to $\tilde{\psi}^{i+\frac{j}{J}}_{mn,q}$ appearing in the inner solution (14). Then ψ becomes continuous at the interfaces. Note that p in the outer region and q in the inner region should be understood to express the same radial location. The remaining condition is the continuity of $\partial\psi/\partial r$ at the interfaces, which is given by

$$\begin{aligned}&\sum_{p=\mathrm{L,R}} \tilde{\psi}^{i+\frac{j}{J}}_{mn,p} (G^{\psi}_{\mathrm{in},mn,p})'(r_q) + (H^{\psi,i+\frac{j}{J}}_{\mathrm{in},mn})'(r_q) \\ &= \sum_{p=\mathrm{L,R}} \tilde{\psi}^{i+\frac{j}{J}}_{mn,p} (G^{\psi}_{\mathrm{out},mn,p})'(r_q), \qquad q = \mathrm{L \text{ or } R},\end{aligned} \tag{17}$$

for each pair of m and n. By solving Eq. (17), we obtain $\tilde{\psi}^{i+\frac{j}{J}}_{mn,p}$. Then we can evaluate the last term of Eq. (14) for the next iteration.

3. Numerical Results

Here we show two kinds of simulation results of magnetic island evolution. The first one is the Rutherford regime of magnetic island evolution in a normal magnetic shear plasma. The second one is the nonlinear evolution of the double tearing mode in a reversed magnetic shear plasma.

3.1 Normal magnetic shear plasma

In this subsection, we take the equilibrium safety factor profile as

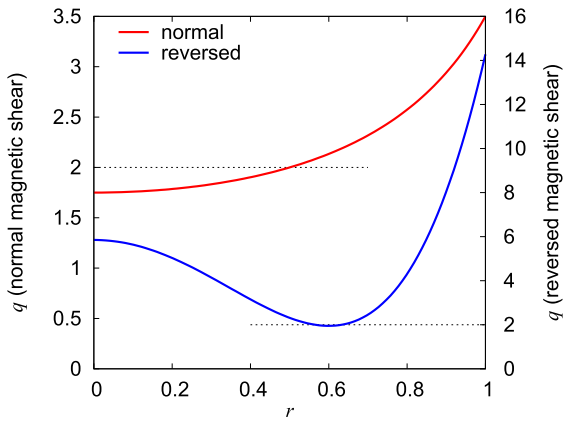

Fig. 1 q profiles used in the numerical demonstrations.

$$q(r) = \frac{q_0}{1 - \dfrac{r^2}{2}}, \tag{18}$$

with $q_0 = 1.75$. Then the $q = 2$ surface exists at $r = 0.5$. The q profile is shown as "normal" in Fig. 1. The other profile will be used in the next subsection. The $m = 2$ and $n = 1$ tearing mode is linearly unstable in this equilibrium; the tearing mode parameter $\Delta'_{m/n=2/1} \simeq 22.4$. The resistivity was chosen to be $\eta = 10^{-6}$. Then the linear growth rate is 2.87×10^{-4} according to the corresponding eigenvalue problem.

In the present study, we only include Fourier components which are resonant at the $q = 2$ surface in the simulations, i.e., a mode family of $m = 2\ell$ and $n = \ell$ with $\ell = 1, 2, \cdots, L$. The maximum number L is chosen to be sufficiently large so that the simulation result does not change much even when L is further increased. For the results shown below, we took $L = 5$. The $m = 0$ and $n = 0$ components are not included in the numerical matching. Thus the equilibrium does not change during the simulation, which is similar to the situation of the Rutherford theory. We also performed fully nonlinear simulations without using the numerical matching for comparison. The $m = 0$ and $n = 0$ components are included for those simulations. In the radial direction, we used the second-order finite difference method. The whole radial domain is divided into a hundred intervals with equal distance in this study. A mesh accumulation is of course possible in principle, or it would be better to do so, in order to increase the resolution inside the inner region. The time integration was performed by the first-order implicit method. The time interval was $h = 0.01$.

Figure 2 shows the time evolution of (a) the kinetic energy E_k and (b) the magnetic energy E_m of the $m = 2$ and $n = 1$ component. Similarly, (c) and (d) show those of the $m = 4$ and $n = 2$ component, and (e) and (f) the $m = 6$ and $n = 3$ component, respectively. Note that the linear eigenmode was used as the initial condition for $m = 2$ and $n = 1$, and that other components were taken to be zero. In the figure, "num. match." denotes our method, and $\Delta r := r_\mathrm{R} - r_\mathrm{L}$ denotes the width of the inner region. The $q = 2$ surface was taken to be at the center of the inner region, thus $r_\mathrm{L} = 0.4$ and $r_\mathrm{R} = 0.6$ for $\Delta r = 0.2$, and $r_\mathrm{L} = 0.3$, $r_\mathrm{R} = 0.7$ for $\Delta r = 0.4$. Also, "full" denotes the result of the fully nonlinear simulation where the resistive reduced MHD equation was solved in the whole domain without the numerical matching. Especially, "full ($m/n = 0/0$ unchanged)" means that the $m = 0$ and $n = 0$ components were held unchanged during the fully nonlinear simulation. This situation is closer to the numerical matching. Also the linear growth is shown in Figs. 2 (a) and 2 (b) by the thin dashed lines. We observe that the energy of the $m = 2$ and $n = 1$ mode grows linearly at the beginning ($t \lesssim 0.3 \times 10^4$), which is followed by the weakly nonlinear or the Rutherford regime. We observe excellent agreement especially between the numerical matching result with $\Delta r = 0.4$ and the fully nonlinear simulation with $m = n = 0$ mode kept unchanged even in the Rutherford regime; those curves are overlapping each other.

On the other hand, the results by the numerical matching, even with $\Delta r = 0.4$, does not agree completely with the "full" result with $m = n = 0$ components being included. This indicates that the inclusion of the $m = n = 0$ components are crucial for achieving quantitative accuracy. This requires further development of the theory.

We also observe that the numerical matching result with $\Delta r = 0.2$ starts to deviate from the "full ($m/n = 0/0$ unchanged)" result around $t \simeq 10^4$. Note that the simulation with $\Delta r = 0.2$ diverged after $t > 1.5 \times 10^4$. The deviation as well as the divergence are because the linear approximation in the outer region starts to break down as the perturbation grows. Indeed, the matching result with the wider inner region $\Delta r = 0.4$ agrees with the full simulation result for longer time.

Figure 3 shows the time evolution of the magnetic island width calculated by the amplitude of the $m = 2$ and $n = 1$ component of ψ. We again observe the excellent agreement between the numerical matching result with $\Delta r = 0.4$ and the full simulation result with $m = n = 0$ mode kept unchanged. We also plotted a simulation result by solving the simplest Rutherford equation $\dfrac{\mathrm{d}w}{\mathrm{d}t} = \eta\Delta'(w)$. The initial island width was taken to be the same as that of the other simulations at $t = 0.3 \times 10^4$. It is not significantly different from our simulation results, except for the $\Delta r = 0.2$ case, although the degree of the agreement may depend on when we start the simulation of the Rutherford equation.

3.2 Reversed magnetic shear plasma

In this subsection, we show one more numerical result. We take the equilibrium safety factor profile with reversed magnetic shear as

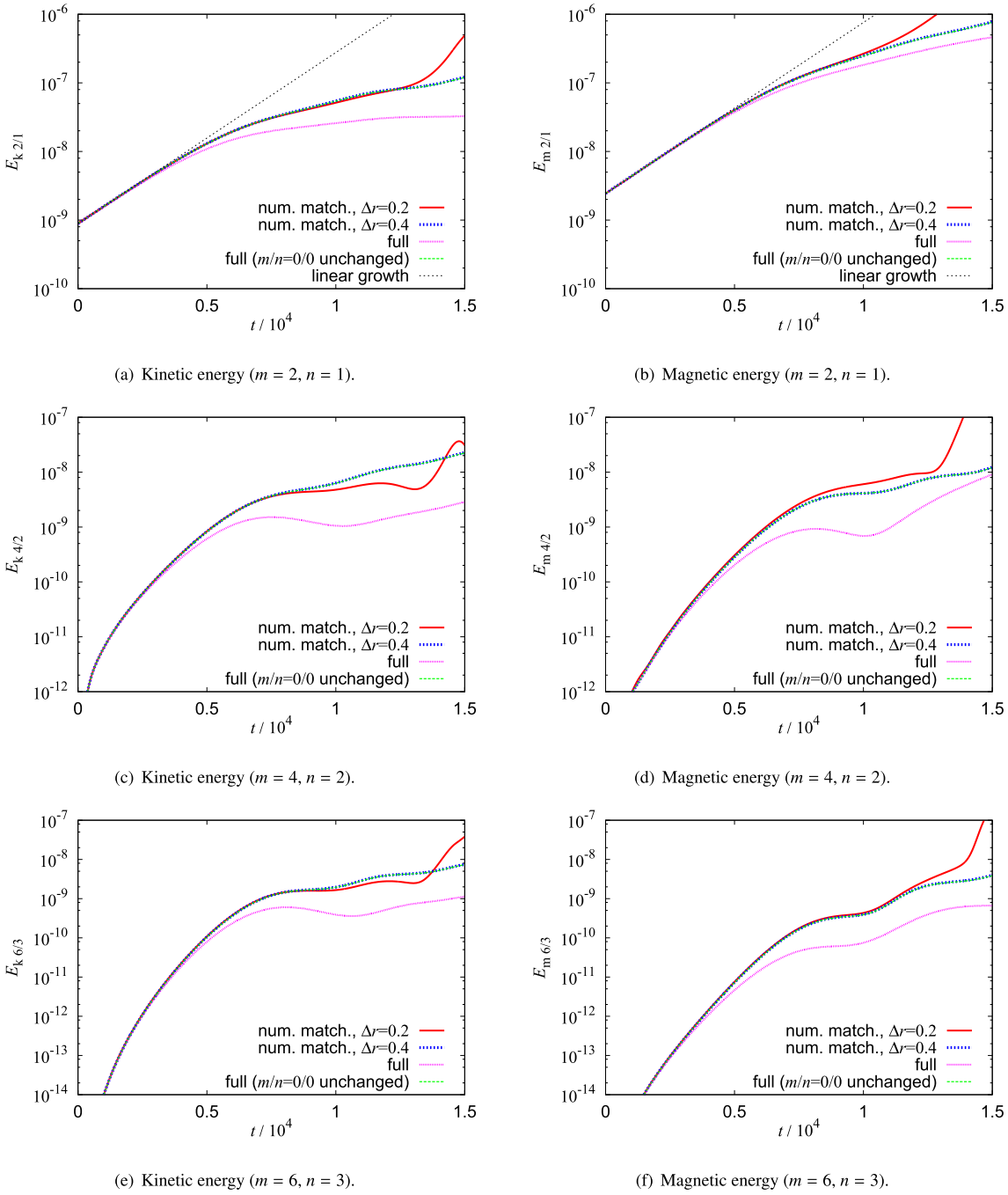

(a) Kinetic energy ($m = 2, n = 1$). (b) Magnetic energy ($m = 2, n = 1$).

(c) Kinetic energy ($m = 4, n = 2$). (d) Magnetic energy ($m = 4, n = 2$).

(e) Kinetic energy ($m = 6, n = 3$). (f) Magnetic energy ($m = 6, n = 3$).

Fig. 2 Time evolution of kinetic and magnetic energy of several Fourier components in the normal magnetic shear plasma. "num. match." denotes our matching method, "full" is the nonlinear simulation in the whole domain without the matching, and "($m/n = 0/0$ unchanged)" means that the $m = n = 0$ components are kept unchanged in the "full" nonlinear simulation. Fourier components of $m = 2\ell$ and $n = \ell$ with $\ell = 1, \cdots, 5$ are included in the simulation, while the $m = n = 0$ components are included only in "full". For "num. match.", Δr means the inner-region width. The matching results, especially with $\Delta r = 0.4$, agree quite well with the full simulation with $m = n = 0$ components kept unchanged for longer time. The linear approximation in the outer region starts to break down for $\Delta r = 0.2$ at $t \gtrsim 10^4$, leading to the deviation from "full".

$$q(r) = q_{\min}\left[(\alpha-1)\left(\frac{r}{r_{\min}}\right)^4 - 2(\alpha-1)\left(\frac{r}{r_{\min}}\right)^2 + \alpha\right], \tag{19}$$

with $q_{\min} = 1.95$, $r_{\min} = 0.6$ and $\alpha = 3$. The q profile is plotted as "reversed" in Fig. 1. There exist two $q = 2$ surfaces around $r = 0.6$. This equilibrium is linearly unstable against the $m = 2$ and $n = 1$ double tearing mode. The resistivity was chosen to be $\eta = 10^{-6}$. Then the linear growth rate is 1.65×10^{-3} according to the corresponding eigenvalue problem. Other parameters for the simulation are the same as in Sec. 3.1 except for the number of the ra-

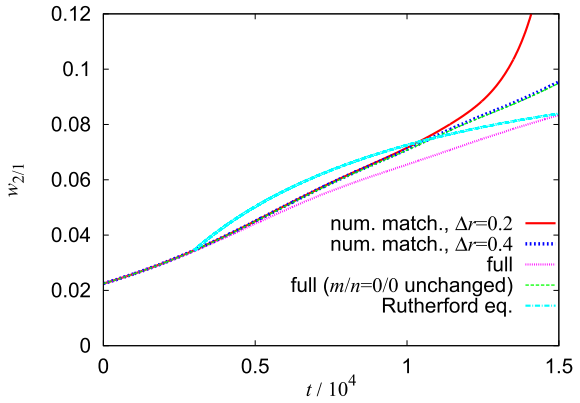

Fig. 3 Time evolution of the magnetic island width. The keys are the same as in Fig. 2. The island width is calculated from the amplitude of the $m/n = 2/1$ component of ψ. Furthermore, numerical solution of the Rutherford equation is also plotted. After the initial linear growth ($t \lesssim 0.3 \times 10^4$), the time evolution enters the Rutherford regime. We observe the good agreement as in the time evolution of energy in Fig. 2.

dial grids; We took two hundred grids with equal spacings in the whole minor radius of the plasma.

Figure 4 shows the time evolution of (a) the kinetic energy E_k and (b) the magnetic energy E_m of the $m = 2$ and $n = 1$ component, (c) and (d) those of the $m = 4$ and $n = 2$ component, and (e) and (f) those of the $m = 6$ and $n = 3$ component, respectively. Because the $q = 2$ surfaces exist near the $q_{\min}$ surface at $r = 0.6$, we took the inner region as $r_L = 0.5$ and $r_R = 0.7$ for $\Delta r = 0.2$, and $r_L = 0.4$, $r_R = 0.8$ for $\Delta r = 0.4$. We observe the good agreement especially between the result of the numerical matching with $\Delta r = 0.4$ and the full simulation with $m = n = 0$ components kept unchanged. The simulation by the numerical matching method with $\Delta r = 0.2$ diverged because of the same reason as in Fig. 2.

4. Discussion

In this section, let us discuss four topics. The first one is the difference concerning the $m = n = 0$ components between the normal and reversed magnetic shear cases shown in the previous section. The second one is the reduction of the computational cost. The third one is the significance of the application to the reversed magnetic shear case, and the last one is the possible application to the high-beta toroidal plasmas.

4.1 Difference of $m = n = 0$ components

In this subsection, we discuss the difference concerning the $m = n = 0$ components between the normal and reversed magnetic shear cases. Comparing these two cases, the deviation from the "full" result, including $m = n = 0$ components, may be larger in the reversed magnetic shear case in Fig. 4 than in the normal magnetic shear case in Fig. 2. This is because the energy of the $m = n = 0$ components is dominant in the reversed magnetic shear case, while it is sub-dominant in the normal magnetic shear case. Figure 5 shows the radial profiles of the real parts of the $m/n = 0/0$ and $2/1$ components of ψ obtained by the fully nonlinear simulation. The imaginary parts are zero. Figures 5 (a) and 5 (b) are the normal and the reversed magnetic shear cases, respectively.

For the normal magnetic shear case in Fig. 5 (a), $t = 5000$ and 15000 are selected as typical timings. The time evolution at $t = 5000$ is the beginning of the nonlinear phase, and $t = 15000$ is much later. As we observe, the $m = n = 0$ component is smaller than the $m = 2$ and $n = 1$ component at both timings. The energy of the $m = n = 0$ components is thus sub-dominant. Because the equilibrium $m = n = 0$ component does not change significantly, the magnetic islands do not saturate even at $t = 15000$.

On the other hand, for the reversed magnetic shear case shown in Fig. 5 (b), we observe that the $m = n = 0$ component is considerably larger than the $m = 2$ and $n = 1$ component at $t = 3500$ which is in the fully nonlinear phase. In the beginning of the nonlinear phase, $t = 1500$, the $m = n = 0$ component is smaller than the $m = 2$ and $n = 1$ component. Thus the energy of the $m = n = 0$ components is dominant at $t = 3500$, which causes the quasi-linear saturation of the double tearing mode in the fully nonlinear phase.

Interestingly, the $m = n = 0$ component is finite within the inner region with $\Delta r = 0.4$ in the reversed magnetic shear case, while it is almost zero in the outer region. Because the $m = n = 0$ component is large in the inner region, the deviation between the numerical results with and without the $m = n = 0$ component is large. However, because the $m = n = 0$ component is localized in the inner region with $\Delta r = 0.4$, the quantitative accuracy can be recovered if the $m = n = 0$ component is also solved only in the inner region of the numerical matching. The Dirichlet boundary condition may be appropriate for the $m = n = 0$ component. For the normal magnetic shear case, on the other hand, the $m = n = 0$ component extends to the outer region, especially at the smaller r region. Because the amplitude of the $m = n = 0$ component is not so large, the deviation between the numerical results with and without the $m = n = 0$ component is smaller. However, we may need to match the $m = n = 0$ component at the interfaces between the outer and the inner regions for this case. The matching of the $m = n = 0$ components requires further development of the theory, which is our future issue.

4.2 Reduction of computational cost

Here we discuss the reduction of the computational cost. Firstly, we note that we should be careful in this comparision because the solution method is totally different. Another point we should consider is that we adopted the first-order implicit time-stepping method for the match-

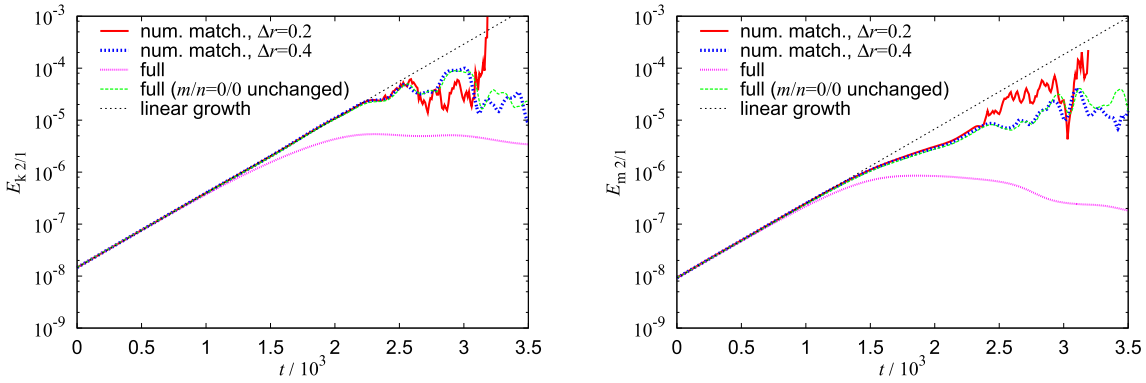

(a) Kinetic energy ($m = 2, n = 1$). (b) Magnetic energy ($m = 2, n = 1$).

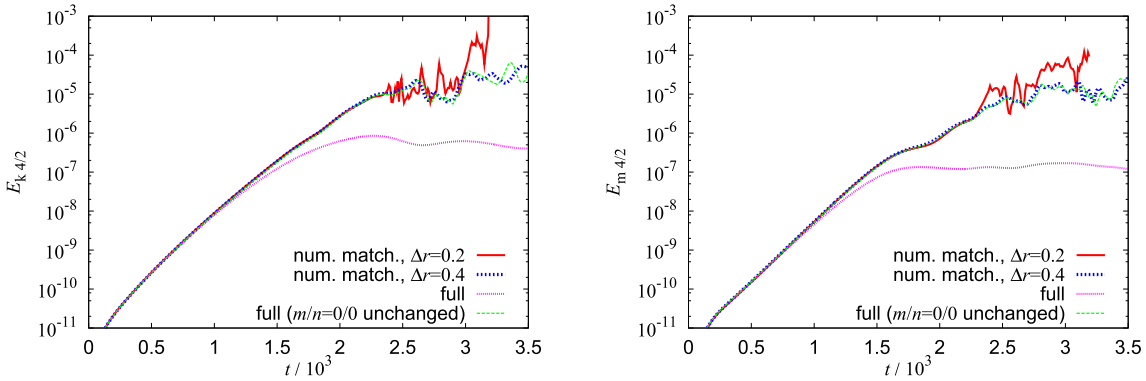

(c) Kinetic energy ($m = 4, n = 2$). (d) Magnetic energy ($m = 4, n = 2$).

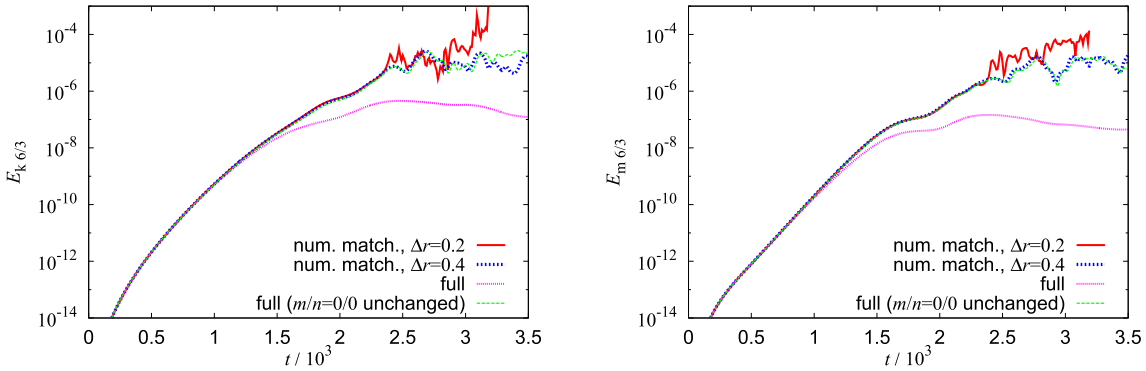

(e) Kinetic energy ($m = 6, n = 3$). (f) Magnetic energy ($m = 6, n = 3$).

Fig. 4 Time evolution of kinetic and magnetic energy of several Fourier components in the reversed magnetic shear plasma. The keys are the same as in Fig. 2. We observe quite good agreement between the numerical matching result with $\Delta r = 0.4$ and the full simulation with $m = n = 0$ components kept unchanged. The simulation with $\Delta r = 0.2$ diverged because of the same reason as in the normal magnetic shear case, i.e., the breakdown of the linear approximation of the outer solution.

ing solutions, while we used the second-order Runge-Kutta method for the full simulation. For this point, we expect that the computational time will not change much for the matching solution even if the second-order algorithm is used, because the formulation is given by the Adams method where the past data required for the next step are stored. Then the computational time for the matching solution with $\Delta r = 0.2$ was about $1/3$ of the full simulation in the numerical example shown in Sec. 3.1. It is not about $1/5$ and thus a bit disappointing. If we develop a method to gradually increase the inner region width as the mode evolves, the computational cost, which gives satisfactory results, will be further reduced.

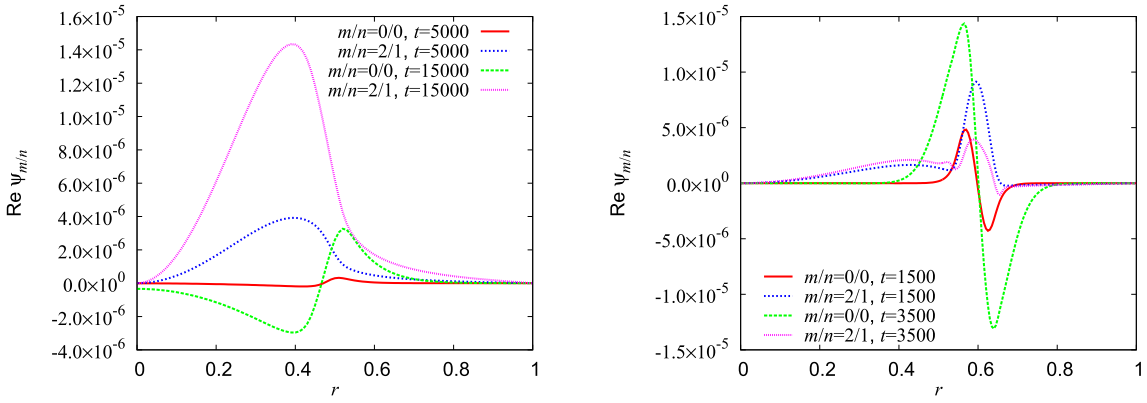

(a) Normal magnetic shear.

(b) Reversed magnetic shear.

Fig. 5 Radial profiles of the real part of ψ for $m/n = 0/0$ and $2/1$ components obtained by the fully nonlinear simulations. (a) and (b) are the normal and the reversed magnetic shear cases, respectively.

4.3 Significance of application to reversed magnetic shear plasmas

Let us here emphasize that our matching method applies even if the magnetic shear vanishes at the $q_{\min}$ surface, e.g. $q_{\min} = 2$ for the $m = 2$ and $n = 1$ mode. The Rutherford theory does not apply to this situation from the beginning. On the other hand, such a q profile can be important in advanced operations. In our previous paper, we have proven that our method calculates the linear stability of this particular situation correctly with no difficulty [6]. Another interesting situation is that the two resonant surfaces are well separated in radius. Then two separated inner regions should be appropriate. Theoretically no difficulty will arise since we only need to match the resonant poloidal Fourier components. This may be different from the case with multiple inner regions in toroidal plasmas, which we will discuss in the next subsection.

4.4 Application to high-beta toroidal plasmas

In this subsection, we discuss application of our matching method to high-beta toroidal plasmas. We have already proven that the numerical matching method can correctly handle the internal kink mode in a cylindrical plasma that simulates the high-beta toroidal plasmas close to the marginal stability [7] because the tearing mode parameter Δ' diverges positively [16] as the internal kink mode. In toroidal plasmas, we need to construct numerically matched solutions using multiple inner regions. Although a prototype of this kind of code has been developed for the linear stability [17], where non-resonant poloidal Fourier components were also matched, the boundary condition for the non-resonant components seems to be more improved.

5. Conclusions

We have extended the numerical matching method to weakly nonlinear cases, which is relevant for the Rutherford regime of magnetic island evolution in normal magnetic shear plasmas as well as for the reversed magnetic shear plasmas to which the Rutherford theory does not apply. We presented two demonstrations of the numerical matching method. One is the Rutherford regime of magnetic island evolution in a normal magnetic shear plasma, while the other is the nonlinear evolution of double tearing mode in a reversed magnetic shear plasma. We observed excellent agreement between the numerical matching results and the fully nonlinear simulations with $m = n = 0$ components kept unchanged. On the other hand we recognized the importance of the $m = n = 0$ components for the quantitative accuracy. The quasi-linear saturation of the double tearing mode in the reversed magnetic shear case may be simulated accurately if the $m = n = 0$ components are solved only in the inner region, because that component is localized in the inner region. Generally, however, we need further development of the theory for including the change of the $m = n = 0$ components for the quantitative accuracy.

Since the nonlinear equation is solved only in the inner region, the computational cost is reduced. Therefore inclusion of detailed physical effects becomes easier because such a model requires more efficient solution method. Our new matching method can simulate the magnetic island evolution continuously from the linear to the weakly nonlinear phases. This cannot be done in the traditional linear and nonlinear (Rutherford) theories based on the matched asymptotic expansion. Furthermore, the Rutherford theory does not apply to the reversed magnetic shear case, which has been simulated by our matching method. Although our method needs further theoretical development, namely its application to the cases with multiple inner regions as well as the mathematical relation to the matched asymp-

totic expansion in a deeper theoretical context, our method will aid understanding physics of MHD activities such as NTMs, and will bring about qualitative changes in MHD analysis of fusion plasmas.

Acknowledgments

This work was supported by KAKENHI Grant No. 23760805 and No. 15K06647.

[1] H.P. Furth, J. Killeen and M.N. Rosenbluth, Phys. Fluids **6**, 459 (1963).
[2] P.H. Rutherford, Phys. Fluids **16**, 1903 (1973).
[3] A.I. Smolyakov, Plasma Phys. Control. Fusion **35**, 657 (1993).
[4] O. Sauter, R.J. La Haye, Z. Chang *et al.*, Phys. Plasmas **4**, 1654 (1997).
[5] R.J. La Haye, Phys. Plasmas **13**, 055501 (2006).
[6] M. Furukawa, S. Tokuda and L.-J. Zheng, Phys. Plasmas **17**, 052502 (2010).
[7] M. Furukawa and S. Tokuda, Phys. Plasmas **18**, 062502 (2011).
[8] M. Furukawa and S. Tokuda, Phys. Plasmas **19**, 102511 (2012).
[9] A. Pletzer and R.L. Dewar, J. Plasma Phys. **45**, 427 (1991).
[10] A. Pletzer, A. Bondeson and R.L. Dewar, J. Comput. Phys. **115**, 530 (1994).
[11] S. Tokuda and T. Watanabe, J. Plasma Fusion Res. **73**, 1141 (1997).
[12] S. Tokuda, Nucl. Fusion **41**, 1037 (2001).
[13] H.R. Strauss, Phys. Fluids **19**, 134 (1976).
[14] H.R. Strauss, Phys. Fluids **20**, 1354 (1977).
[15] W.A. Newcomb, Ann. Phys. **10**, 232 (1960).
[16] D.P. Brennan, E.J. Strait, A.D. Turnbull, M.S. Chu, R.J. La Haye, T.C. Luce, T.S. Taylor, S. Kruger and A. Pletzer, Phys. Plasmas **9**, 2998 (2002).
[17] M. Furukawa, The 32th Annual Meeting, the Japanese Society of Plasma and Nuclear Fusion Research, 2015, 26aE02P.